AIAA JOURNAL
Vol. 31, No. 12, December 1993

Experiments in Nonreacting Compressible Shear Layers

J. L. Hall,* P. E. Dimotakis,† and H. Rosemann‡
California Institute of Technology, Pasadena, California 91125

Two-dimensional, compressible turbulent shear layers are studied in a new wind-tunnel facility. Helium, nitrogen, and argon gases are used in various combinations to produce shear layers with isentropically computed convective Mach numbers that range from near zero to unity. Side-view schlieren photographs of these compressible flows are generally devoid of the two-dimensional, large-scale structures seen in incompressible flows. Traveling shock and expansion waves are observed in the high-compressibility flows, evidently created by turbulent structures convecting at supersonic velocities with respect to one of the freestreams. Such waves are seen only in the low-speed fluid, with apparent convection velocities much higher than those predicted by the usual isentropic pressure-matching arguments. The measured shear layer growth rates agree with previous results by other experimenters, except for a few unusual cases at low compressibility and low-density ratio. Finally, it is observed that shear layer growth rate is relatively insensitive to the effects of incident shock and expansion waves on the shear layer.

Nomenclature

a_1, a_2 = static sound speeds of the high- and low-speed freestreams, respectively
M_1, M_2 = Mach number of the high- and low-speed freestreams, respectively
M_{c1} = convective Mach number of structures moving with respect to the high-speed stream
M_{c2} = convective Mach number of structures moving with respect to the low-speed stream
$M_{cj}^{(i)}$ = predicted value for convective Mach number of stream j based on the isentropic model
M_s = shock Mach number
p_1, p_2 = static pressure of high- and low-speed freestreams, respectively
r = velocity ratio u_2/u_1
Re_x = shear layer Reynolds number based on downstream distance
Re_δ = shear layer Reynolds number based on local visual thickness
s = density ratio ρ_2/ρ_1
T_1, T_2 = static temperatures of the high- and low-speed freestreams, respectively
u_c = convection velocity of large-scale structures
u_1, u_2 = velocities of the high- and low-speed freestreams, respectively
ΔU = velocity difference across the shear layer, $(u_2 - u_1)$
x = distance downstream from the splitter tip
α_1, α_2 = orientation angles of high- and low-speed shear layer edges, respectively
β = lower guidewall convergence angle
γ_1, γ_2 = ratio of specific heats of high- and low-speed streams, respectively
δ_{vis} = visual thickness of the shear layer
μ = wave angle of oblique waves in the flow
ν = kinematic viscosity
ρ_1, ρ_2 = static densities of the high- and low-speed freestreams, respectively
$(\ )_{inc}$ = parameter estimated using an incompressible model

Presented as Paper 91-0629 at the AIAA 29th Aerospace Sciences Meeting, Reno, NV, Jan. 7–10, 1991; received June 26, 1991; revision received Nov. 12, 1992; accepted for publication Nov. 16, 1992.

*Graduate Student, Graduate Aeronautical Laboratories; currently Research Associate, Cryofuel Systems, U. Victoria, Canada. Member AIAA.

†Professor, Aeronautics and Applied Physics, Graduate Aeronautical Laboratories. Associate Fellow AIAA.

‡Research Fellow in Aeronautics, Graduate Aeronautical Laboratories; currently Research Scientist, DLR, Göttingen, Germany.

Introduction

THERE has been considerable experimental activity in the field of compressible turbulent shear layers in recent years,[1-7] partly inspired by the effort to develop scramjet engine technology. This activity is also motivated by the desire to understand compressible turbulent shear flows in the context of the coherent structure models that have been developed for incompressible shear layers over the past 20 years. The work reported here can be viewed as a logical extension of this effort.

Currently available experimental evidence for large-scale structures in compressible shear layers is not definitive. Most of the available schlieren photographic data, for example, do not clearly show the two-dimensional coherent structures seen in incompressible flows.[1,2] Recent pictures by Clemens and Mungal,[4] however, do show such structures, if only at rather low compressibility levels. Further evidence for coherent structures can be found in the axisymmetric jet experiments of Fourguette et al.[6] Their planar, Rayleigh scattering images show distinct regions of fluid separated by regular intervals. Interestingly enough, this structure was detected at a compressibility level beyond that at which Clemens and Mungal reported such structures.[4] In view of the role played by three-dimensional effects in compressible turbulent shear layers, the difference between a "slice" view (e.g., planar Rayleigh scattering image) and a spanwise integrated view (e.g., schlieren) can potentially account for this difference.

The convective Mach number measurements of Papamoschou[3] present us with another, at best only partially resolved, issue for compressible shear layers. Papamoschou used double-spark schlieren photography to track turbulent features in the flow and thereby to infer the large structure convection velocity u_c. From these measurements, he was able to estimate the convective Mach numbers for the flow, i.e.,

$$M_{c1} \equiv \frac{u_1 - u_c}{a_1} \quad \text{and} \quad M_{c2} \equiv \frac{u_c - u_2}{a_2} \tag{1}$$

where u_j and a_j are the freestream velocities and sound speeds in the jth freestream, respectively. His results, as well as one point computed from the data of Fourguette et al.,[6] are plotted in Fig. 1. It can be seen that, for high-convective Mach numbers, the measured convection velocities tend to be close to one freestream velocity or the other, resulting in one low- and one high-convective Mach number.

These results are not in accord with theoretical estimates of the convective Mach number based on isentropic pressure recovery at the large-scale structure interstitial stagnation points, in the convective frame of reference.[2,8-10] Specifically, pressure matching at these points, with isentropic pressure recovery, requires

$$p_1\left(1+\frac{\gamma_1-1}{2}M_{c1}^2\right)^{\gamma_1/(\gamma_1-1)}=p_2\left(1+\frac{\gamma_2-1}{2}M_{c2}^2\right)^{\gamma_2/(\gamma_2-1)} \quad (2)$$

where p_j is the static pressure and γ_j is the ratio of specific heats in the jth freestream. For $p_1=p_2$ and $\gamma_1=\gamma_2$, this yields $M_{c1}=M_{c2}$. Furthermore, it is easy to appreciate that M_{c1} and M_{c2} remain fairly close even when $\gamma_1\neq\gamma_2$, provided that $p_1\simeq p_2$, as is usually the case in such experiments.

The convection velocity measurements of Papamoschou[3] then suggest that grossly unequal total pressure losses must occur on the two sides of the shear layer, if the requirement of a pressure balance at the convective-frame stagnation points is to be observed. This led both Papamoschou[3] and Dimotakis[11] to speculate that shock waves are generated by turbulent structures on only one side of the shear layer in these flows, thereby providing a mechanism for unequal total pressure losses. A subsequent model by Dimotakis[12] yielded a procedure capable of quantitative predictions of the convective Mach number based on the freestream flow parameters. The strong shock waves assumed in these models, however, had not been detected in a shear layer experiment before the work reported here.

The present experiments were designed to address these issues, as well as to provide growth rate data that could be compared with previous results from other experimenters.[1,2,4] To this end, a new, short-running-time, blowdown wind-tunnel facility was developed, which will be briefly described in the next section. The new experimental data will then be presented and discussed.

Experimental Facility and Diagnostics

The experiments reported here were performed in the new GALCIT supersonic shear layer combustion facility (Fig. 2). This is a two-stream blowdown wind tunnel, with a nominal run time of 3 s. It was designed to accommodate chemically reacting flows based on $H_2/F_2/NO$ chemistry. The results reported here, however, are entirely based on nonreacting experiments. For this work, the facility was configured for a supersonic high-speed stream, $M_1\simeq 1.5$, and a subsonic low-speed stream, $M_2<0.5$. Different convective Mach numbers were generated primarily by using different gas combinations in the two freestreams. The static pressure of the shear layer was nominally 1 atm.

For these experiments, the desired gases or gas mixtures were loaded into a pair of storage tanks. At run time, parallel piping networks delivered these gases to the test section via shutoff and flow regulating valves. Inside the test section (Fig. 3) the gases flowed through screens, honeycomb, and appro-

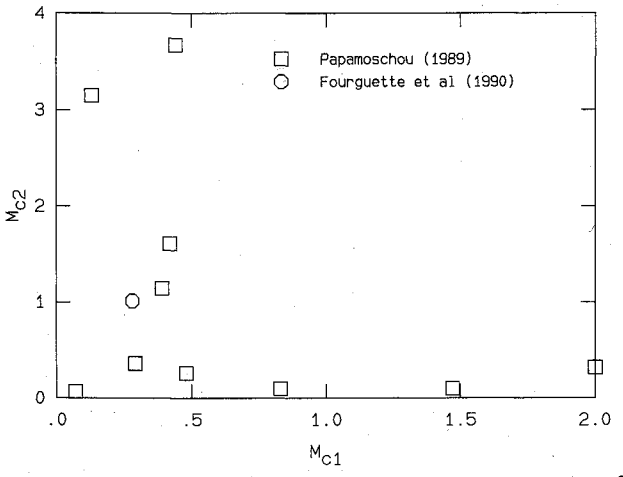

Fig. 1 Unequal convective Mach numbers measured by Papamoschou[3] and Fourguette et al.[6]

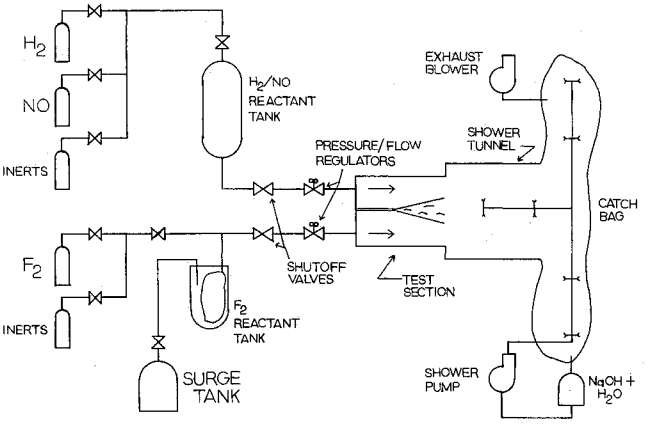

Fig. 2 Flow schematic of the supersonic shear layer combustion facility.

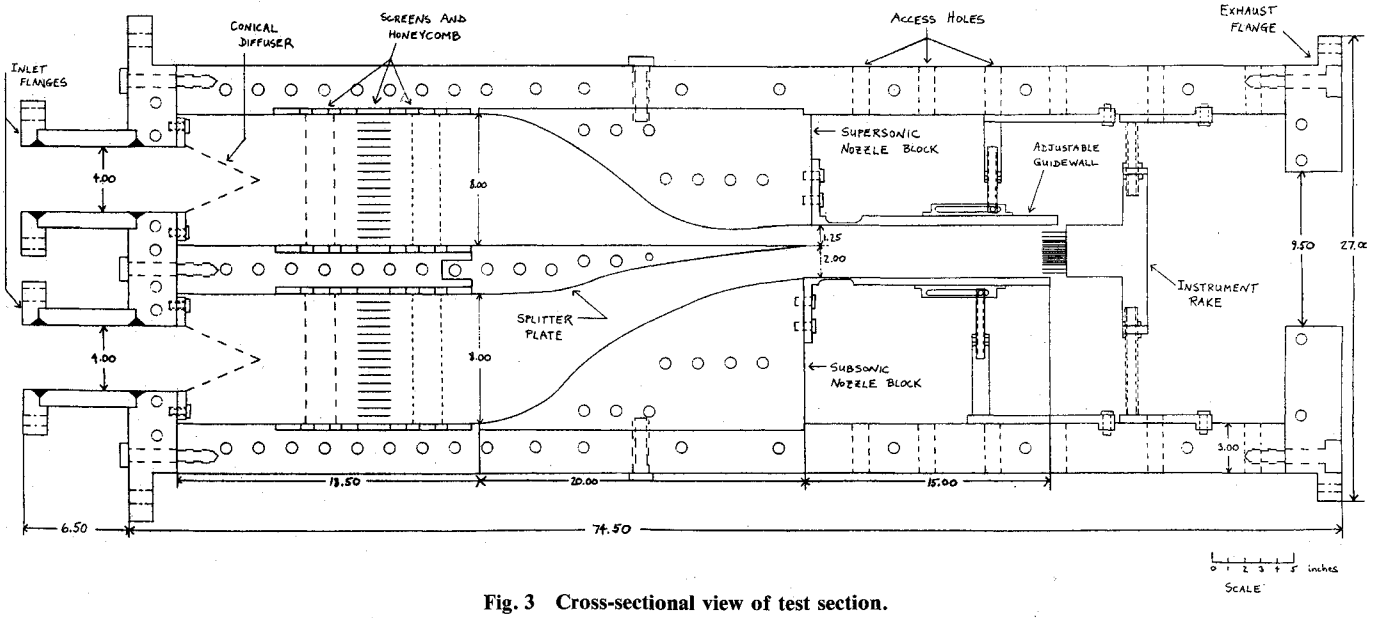

Fig. 3 Cross-sectional view of test section.

priately contoured two-dimensional nozzles before coming into contact at the end of the splitter plate. The shear layer formed between the two freestreams, confined by adjustable guidewalls on the top and bottom and two windows on the sides. Upon exiting the test section, the shear layer gases entered a waste gas disposal system.

For the experiments reported here, the test section flow diagnostics were comprised of the following elements: 1) side-view schlieren photography, 2) guidewall static pressure transducers (6 per wall), 3) cross-stream total pressure tubes (16 in all), and 4) cross-stream exposed junction thermocouples (16 in all).

With the exception of the schlieren photography and some of the guidewall pressure transducers, these diagnostics were fairly low-frequency response sensors primarily used for time-averaged measurements. The schlieren system spark source had a 20-ns pulse duration, which was sufficiently fast to freeze the flow. The few fast guidewall pressure transducers were 1-MHz piezoelectric devices that were also capable of temporally resolving the flow. Further details on the facility design and operation can be found in Hall.[13]

Results and Discussion

Figure 4 shows the basic geometry and coordinate system for the shear layer flows that will be discussed here. Stream 1 is defined as the high-speed stream with velocity u_1, density ρ_1, pressure p_1, temperature T_1, Mach number M_1, and specific heat ratio γ_1. The same variables are used on the low-speed side with a subscript 2. The upper (high-speed) guidewall bounding the flow is parallel to the x axis. The lower guidewall is deflected through an angle β to control the streamwise pressure gradient dp/dx. The angles α_1 and α_2 denote the orientation of the corresponding shear layer edges within the channel. In this study, the shear layer thickness δ corresponds to the visual thickness as measured from schlieren photographs.

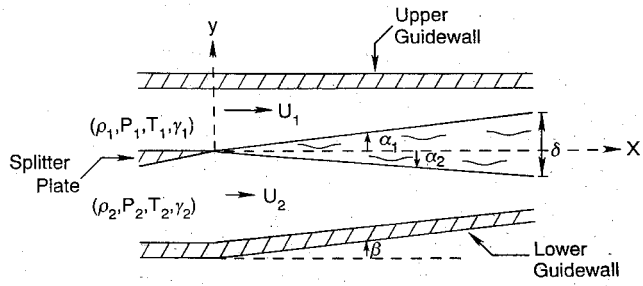

Fig. 4 Shear layer geometry.

The two-dimensional nozzle contours for the two gas streams were designed to produce uniform velocity profiles at the splitter tip location. Pitot measurements on the low-speed side confirmed the flow uniformity to $\pm 1\%$ of the freestream velocity. Flow uniformity on the high-speed side was confirmed by the absence of strong Mach waves emanating from the nozzle (e.g., Figs. 5, 10, and 11). The boundary layer on the high-speed side at the splitter tip location is calculated to be turbulent ($Re_x \sim 10^6$), with a displacement thickness of roughly 0.5 mm. Note that the splitter tip itself consists of a 5-deg convergence angle with a trailing-edge radius of $\simeq 0.25$ mm.

A list of the experiments to be discussed can be found in Table 1. The test cases are listed in order from highest to lowest compressibility, as determined by the isentropic pressure-matching model value for M_{c1} [Eq. (2)]. The values for $(\delta/x)_{inc}$ are estimated using the expression proposed by Brown,[14] i.e.,

$$\left(\frac{\delta}{x}\right)_{inc} \simeq C_\delta \frac{(1-r)(1+s^{1/2})}{1+rs^{1/2}} \tag{3}$$

where $r \equiv u_2/u_1$ is the velocity ratio, $s \equiv \rho_2/\rho_1$ is the density ratio, and C_δ is a constant, here given the value of 0.17 (Ref. 2). It is noted here that the expression given by Brown[14] is for a temporally growing shear layer. It is used here, as opposed to an expression for a spatially growing shear layer, to provide a direct comparison with previous, similarly compiled, data. An estimate for a spatially growing layer growth can be made by multiplying the expression in Eq. (3) by the (near-unity) factor,

$$\frac{(\delta/x)_{spatial}}{(\delta/x)_{temporal}} \simeq 1 - \frac{(1-s^{1/2})/(1+s^{1/2})}{1+2.9(1+r)/(1-r)} \tag{4}$$

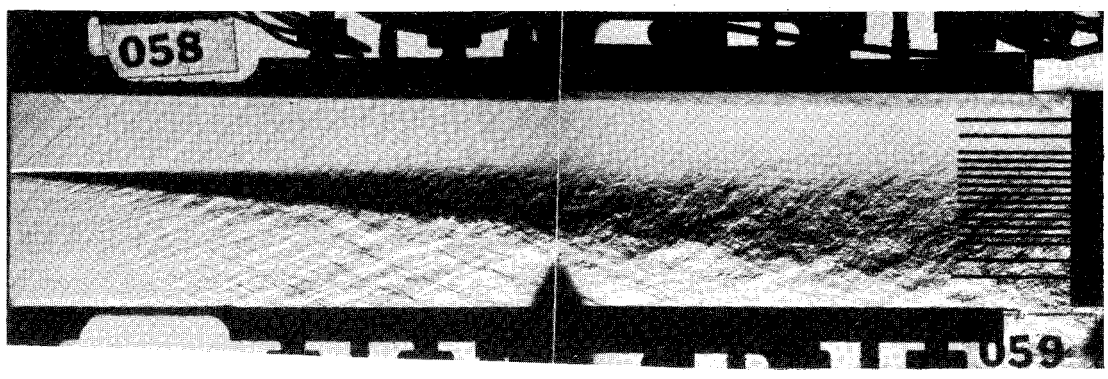

Fig. 5 Side-view schlieren photograph of case 1 (He/Ar) flow.

Table 1 Summary of test cases

Case	1	2	3	4	5	6	7	8	9	10	11
Stream 1	100% He	100% He	100% N_2	100% N_2	100% N_2	100% N_2	100% N_2	100% N_2	100% Ar	100% N_2	100% N_2
Stream 2	100% Ar	100% N_2	100% N_2	33% He 66% Ar	60% He 40% Ar	75% He 25% Ar	90% He 10% Ar	100% He	100% He	33% He 66% Ar	100% He
M_1	1.50	1.48	1.46	1.48	1.48	1.47	1.48	1.48	1.50	0.59	0.65
M_2	0.35	0.30	0.29	0.44	0.42	0.36	0.28	0.23	0.23	0.27	0.10
$r = u_2/u_1$	0.096	0.092	0.24	0.39	0.45	0.46	0.47	0.51	0.64	0.51	0.46
$s = \rho_2/\rho_1$	5.95	4.12	0.71	0.71	0.48	0.34	0.19	0.10	0.058	0.96	0.13
$M_{c1}^{(i)}$	0.96	0.91	0.51	0.43	0.34	0.29	0.24	0.18	0.11	0.14	0.093
$(\delta/x)_{inc}$	0.43	0.40	0.20	0.15	0.12	0.12	0.11	0.094	0.067	0.11	0.11
$(\delta/x)_{vis}$	0.10	0.11	0.11	0.092	0.083	0.084	0.073	0.062	0.040	0.10	0.097
$\delta_{vis}/\delta_{inc}$	0.23	0.27	0.57	0.63	0.68	0.73	0.68	0.66	0.60	0.92	0.901
Re_x	2.2×10^7	1.8×10^7	1.1×10^7	8.4×10^6	6.3×10^6	5.5×10^6	4.9×10^6	4.2×10^6	4.3×10^6	2.3×10^6	1.7×10^6
β, deg	0	1	2	0	0.5	0.5	1	2	2	0.5	1

See Refs. 9 and 11, Fig. 1, and associated discussion for more details. Finally, the Reynolds number

$$Re_x \equiv \frac{\Delta U x}{\nu} \tag{5}$$

where $\Delta U \equiv u_2 - u_1$ is the velocity difference across the layer and is estimated with ν as the average kinematic viscosity of the two freestreams, i.e., $\nu \equiv (\nu_1 + \nu_2)/2$, and x is the streamwise distance from the splitter tip to the cross-stream instrument rake. (For the experiments reported here, $x = 0.38$ m.)

A horizontal knife edge schlieren photograph of the highest compressibility flow (case 1) appears in Fig. 5. Immediately obvious is a complex yet regular wave system in the low-speed flow. This is a traveling wave system created by shear layer structures that are convecting supersonically with respect to the low-speed stream. Note that they cannot be standing waves (as are seen in the high-speed flow near the nozzle exit) because $M_2 \ll 1$. Upon close inspection, the wave system is seen to be comprised of a set of waves originating at the shear layer and a set of reflected waves off the lower guidewall. Each set is composed of alternating compression and expansion waves, which must nearly balance each other to maintain a negligible streamwise pressure gradient. The incident wave system is reminiscent of those seen in the supersonic jet experiments of Lowson and Ollerhead,[15] Tam,[16] and Oertel[17] and is presumably of the same origin.

It is not possible to discern on the basis of Fig. 5 the precise nature of the shear layer structures that created the traveling waves. In fact, the shear layer seems devoid of any kind of spanwise-coherent large-scale structure. Nevertheless, the characteristic spacing of the traveling waves is seen to be on the order of the local shear layer thickness δ_{vis}, suggesting that some form of large-scale structure is present. Further attempts were made to image this large-scale structure by desensitizing the schlieren system and by rotating the knife edge to the vertical position. None of the photographs from these experiments, however, revealed any more large-scale structure than is seen in Fig. 5. There are at least two possible explanations for this result: the large-scale structure is highly distorted by spanwise three dimensionality, or the large-scale structure is obscured by the signal from many small-scale, high-gradient turbulent interfaces superimposed on it. However, it is not possible to choose between these possible explanations on the basis of the available data.

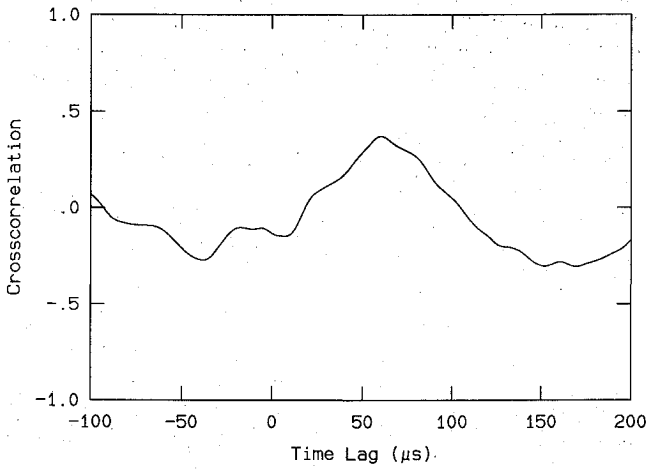

Fig. 6 Cross correlation of guidewall pressure transducers.

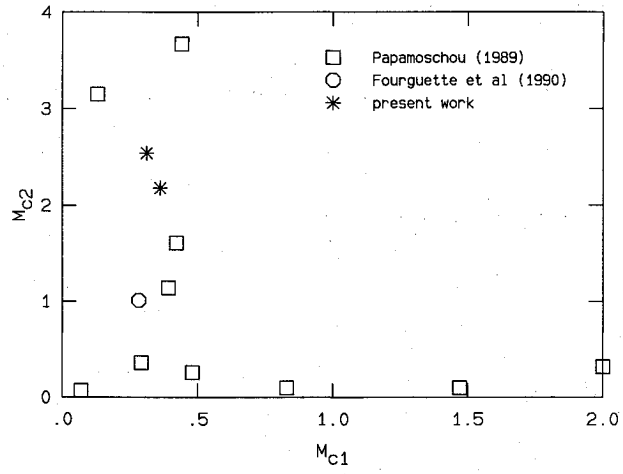

Fig. 7 Measured convective Mach numbers plotted with other available data.

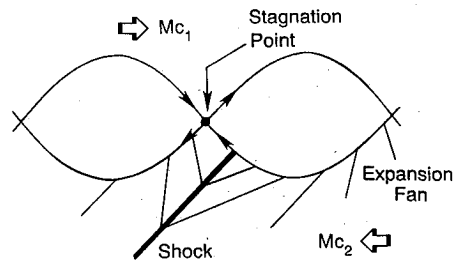

Fig. 8 Model for shear layer recompression shock (Papamoschou[3]).

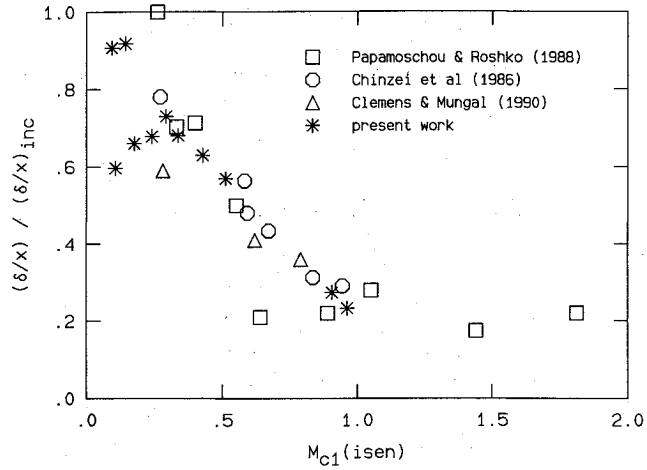

Fig. 9 Normalized growth rate of all cases plotted with other available data.

Despite the lack of observed structure, the traveling waves strongly suggest that there is a well-defined convection velocity for the fluid inside the shear layer. Specifically, the wave angles of these waves are tightly clustered in the range of $23 < \mu < 28$ deg, where μ is measured with respect to an imaginary line that roughly bisects the shear layer wedge. This direction is an estimate for the direction of travel of the wave-creating structures in the shear layer. These wave angles provide a direct estimate of the convective Mach number for this flow, i.e.,

$$M_{c2} \simeq \frac{1}{\sin \mu} \tag{6}$$

The range of wave angles quoted earlier yields $2.1 < M_{c2} < 2.6$ for this case 1 flow.

This Mach number range is also corroborated by static pressure measurements made on the low-speed guidewall. Specifically, two piezoelectric pressure transducers spaced 5 cm apart were used to track the pressure "footprint" of the traveling waves. A cross correlation of the two pressure signals (Fig. 6) shows a peak centered at 59 μs, which translates into a convective Mach number of $M_{c2} \simeq 2.54$.

This experimentally inferred value is very different from the isentropic pressure-matching value of $M_{c1}^{(i)} \simeq 1$ (Table 1). Note that, given $M_{c2} \simeq 2.54$, Eq. (1) requires that $M_{c1} \simeq 0.31$. This provides a strong corroboration of the Papamoschou[3] results that indicated very different convective Mach numbers for high-compressibility flows. The results for cases 1 and 2, the only flows to exhibit traveling waves, are plotted in Fig. 7, along with the Papamoschou[3] and Fourguette et al.[6] data. The present data are in accord with previous measurements, confirming the convective Mach number asymmetry for high-compressibility shear layers.

There remains a problem, however, in that the observed traveling waves are too weak to completely fulfill the pressure dissipation role required to reconcile the stagnation point, pressure-matching model with the measured convection velocities. The agreement between the wave angle and pressure cross-correlation measurements suggests that the observed waves are weak. Furthermore, a normal shock wave with a shock Mach number of $M_s = M_{c2} = 2.54$ in case 1, for example, cannot dissipate enough total pressure to satisfy the requirement. A possible resolution of this dilemma can be found in the idea that shear layer vortices may be capable of locally accelerating the flow to Mach numbers much higher than M_{c2} (Refs. 3 and 12). Such accelerated flow must eventually come to rest at the stagnation point in the convective reference frame (Fig. 8), a process that will require one or more recompression shocks within the shear layer region. One can readily calculate that if this recompression process were modeled as a single normal shock, then satisfying the pressure dissipation requirement for this flow results in a shock Mach number of

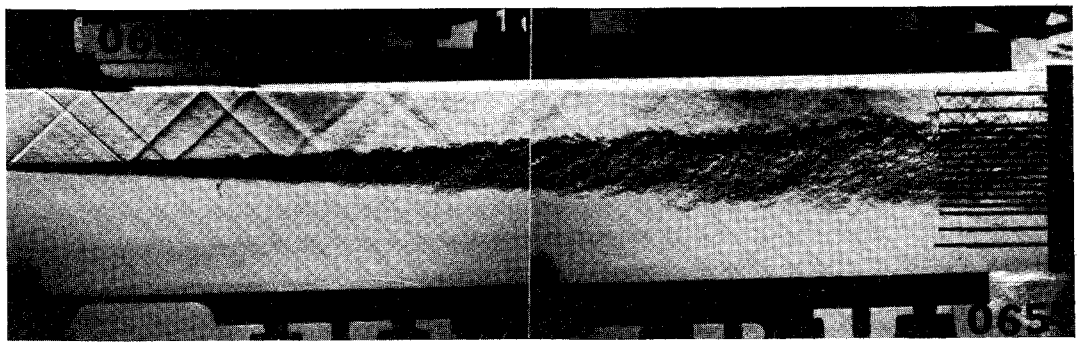

Fig. 10a Side-view schlieren photograph of case 6 flow.

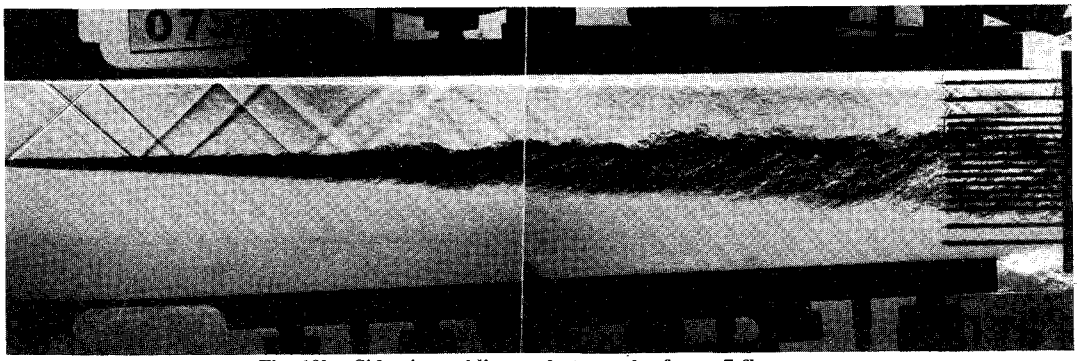

Fig. 10b Side-view schlieren photograph of case 7 flow.

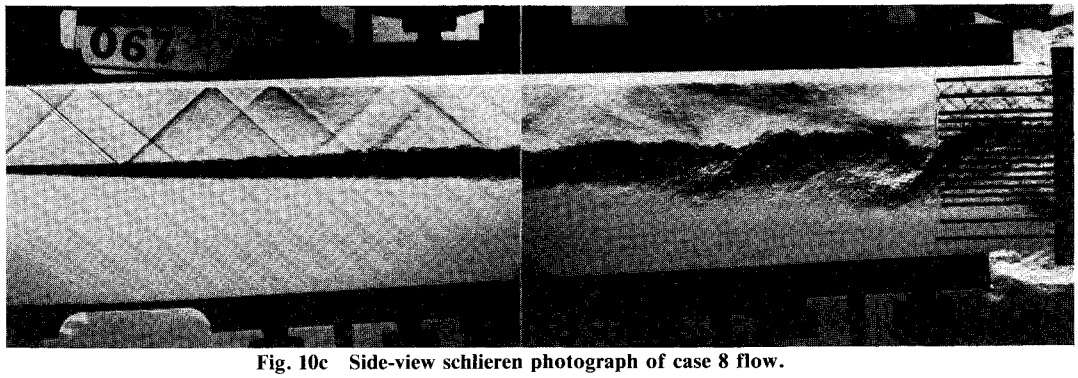

Fig. 10c Side-view schlieren photograph of case 8 flow.

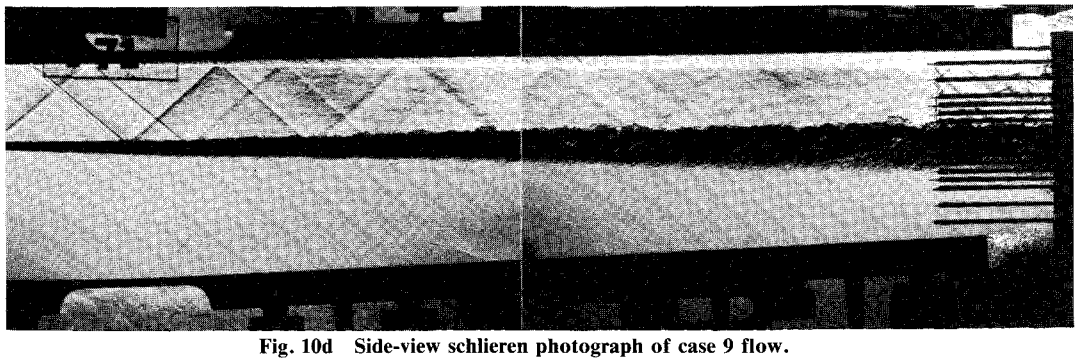

Fig. 10d Side-view schlieren photograph of case 9 flow.

approximately 7. Such a strong recompression shock was not detected in any experiment to date. This includes several experiments reported in this effort that tried imaging using a variety of knife edge configurations. It should be noted, however, that the recompression process inside the shear layer may consist of several weaker oblique shocks rather than a single normal shock.[12] These oblique shocks would be more difficult to detect in schlieren photographs. Alternatively, it is conceivable that the same elements that potentially prevent detection of large-scale shear layer structures (three dimensionality and superimposed small-scale turbulence) also hide embedded shock waves. Nevertheless, given the very large pressure dissipation requirements, it is arguably surprising that such dissipative shocks do not show up in the available schlieren photographs.

Cases 1 and 2 were the only flows to exhibit the traveling waves. Figure 10a is a schlieren photograph of a typical, moderate-compressibility flow, $M_{c1}^{(i)} \simeq 0.29$, illustrating the absence of both traveling waves and of apparent large-scale structure.

The normalized growth rates for all 11 cases in the current study are plotted vs the isentropically computed convective Mach number $M_{c1}^{(i)}$ in Fig. 9, along with data from other researchers. Note that the measured growth rate (δ_{vis}/x) has been normalized by the estimated incompressible growth rate, as given by Eq. (3). For $M_{c1}^{(i)} > 0.3$, the collapse of the data is seen to be quite good. There is a clear trend toward lower growth rates at high compressibility. This experimentally observed trend is also supported by the results from linear stability theory (e.g., Refs. 18–22), although the quantitative predictions of growth rate decrease are somewhat dependent on the details assumed for the flow. The collapse of the experimental data is somewhat surprising, given the results already discussed for the high-compressibility cases, which indicate that the measured convective Mach number is very different from $M_{c1}^{(i)}$. Perhaps this can be understood by considering $M_{c1}^{(i)}$ to be an *average* measure of compressibility in the flow, a parameter that, using the case 1 flow as an example, combines the effects of a supersonic M_{c2} and a subsonic M_{c1}. The value of $M_{c1}^{(i)}$ is also close to the parameter $\Delta U/(a_1 + a_2)$ suggested by Papamoschou[3] as a means of determining when compressibility effects become important in the flow. From this point of view, $M_{c1}^{(i)}$ may still be a valid measure of the overall compressibility of the shear layer, although the underlying physical ideas are somewhat different than originally thought.

As can be seen, however, the data do not collapse at all for $M_{c1}^{(i)} < 0.3$. The results for the current experiments are particularly unusual, with cases 7–9 forming a trend of growth rate *reduction* at very low-compressibility levels. This reduction is particularly surprising considering the all-subsonic flows of cases 10 and 11 that almost recover the theoretical incompressible growth rate despite having the same value of $M_{c1}^{(i)}$ as cases 8 and 9. It should be noted that the only real difference between these pairs of flows is the existence of $M_1 > 1$ in cases 8 and 9 vs $M_1 < 1$ in cases 10 and 11. The Reynolds number Re_x, the velocity ratio r, and the density ratio s (case 10 excluded) are all roughly the same for these flows.

Further clues to this unusual behavior can be gleaned from the schlieren photographs of cases 6–9 (Fig. 10). The case 6 photograph (Fig. 10a) shows the flow before the growth rate reduction trend starts. Note the apparent absence of large-scale coherent structures. In cases 7 and 8, however, one can detect some structure, particularly in the downstream section of case 8. Curiously enough, there are no large-scale structures in the case 9 flow, although the growth rate reduction is quite pronounced. Taken together, this sequence of flows of decreasing $M_{c1}^{(i)}$ suggests that a change in shear layer behavior is taking place, one accompanied by shear layer thinning and the formation of some detectable structure at the downstream end.

Very little is known about this behavior, except that it coincides with very low-density ratios. The density ratios for cases 7–9 are in fact lower than any of the other compressible flows represented in Fig. 11. Such low-density ratios were a necessary byproduct of the methodology of producing low $M_{c1}^{(i)}$ flows by increasing the helium content of the low-speed fluid and hence increasing its sound speed. Note that a low-density ratio, by itself, does not result in abnormally low growth rates; witness the case 11 flow result in this study and the previous low-density, incompressible results of Brown and Roshko[23] and Frieler and Dimotakis.[24] Only the coupling of a low-density ratio and a supersonic freestream Mach number

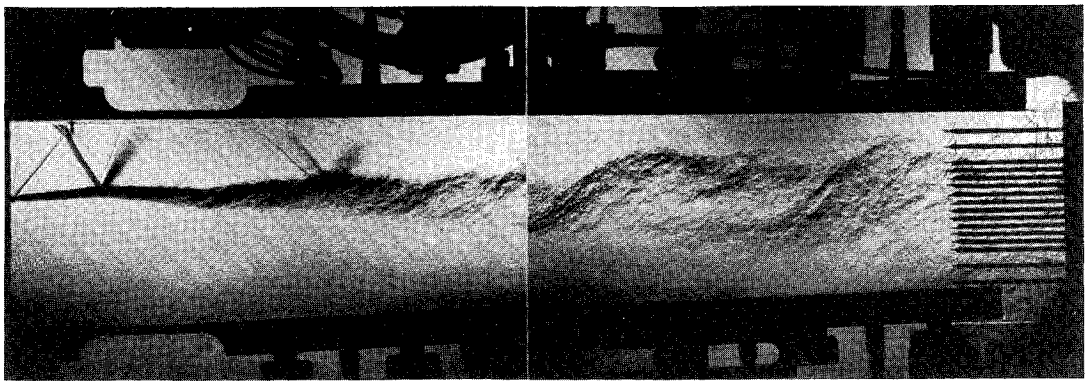

Fig. 11a Side-view schlieren photograph of an off-design case 3 flow showing growth rate insensitivity.

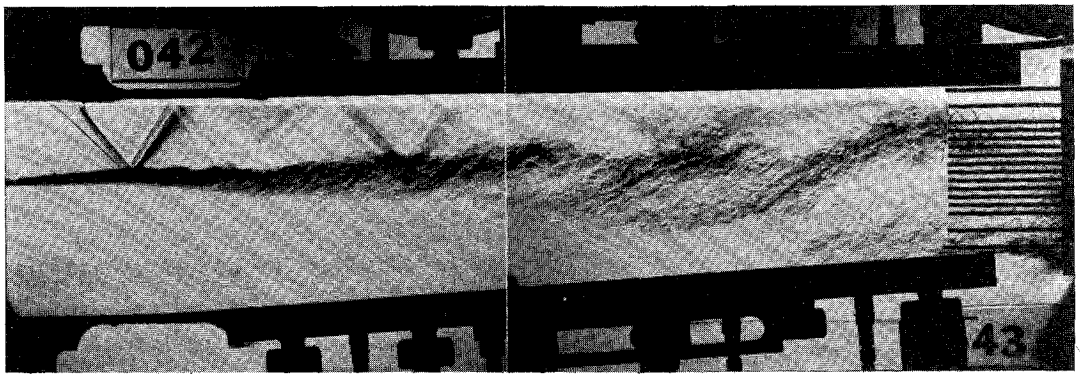

Fig. 11b Side-view schlieren photograph of an off-design case 3 flow showing structure enhancement.

seems to result in these low growth rates. One might reasonably suspect that the hyperbolic character of the $M_1 > 1$ freestream flow lies at the heart of the matter. Certainly, this will inhibit downstream-to-upstream feedback mechanisms in the flow.[11,25] Of course, such inhibition is present whether the flow possesses a low-density ratio or not.

One can speculate that a new growth rate mechanism is in effect for these low-density, supersonic high-speed stream flows. This mechanism first becomes important in case 7, indicating the start of the new behavior, and it evidently dominates the shear layer growth rate in the case 9 flow. Note that this new growth rate mechanism does not appear to be related to the so-called "wake effect" identified by Koochesfahani and Frieler.[26] They found that a second instability mode becomes important, one that is related to the momentum deficit in the wake of the splitter tip, in addition to the usual Kelvin-Helmholtz instability, at *high*-density ratios ($s \geq 6$).

The potentially different structure that may characterize the flow for low freestream density ratios could result in incompressible shear layer growth rates that are not well represented by the expression in Eq. (3). Lu and Lele[27] report good collapse of compressible shear layer data, throughout the density ratio range, if the compressible shear layer growth rate normalization is based on a growth rate for the corresponding incompressible flow derived on the basis of linear stability analysis.[27] Interestingly, Eqs. (3) and especially (4) provide a better representation of the freestream density ratio dependence of the documented growth rates δ_{vis}/x for incompressible shear layers (cf. Ref. 11, Fig. 1) than stability analysis predictions. Nevertheless, cases 8 and 9 are at freestream density ratios ($\rho_2/\rho_1 = 0.10$ and 0.058, respectively) that fall outside the incompressible experimental data base, and the possibility of a qualitative departure in behavior cannot be ruled out at this time.

The final results to be discussed here concern two off-design flows based on the medium compressibility case 3 condition. The first flow (Fig. 11a) demonstrates the relative insensitivity of the overall growth rate to the impact of a strong planar wave. This wave is created at the splitter tip by a large pressure mismatch between the freestream static pressures at this point. The wave subsequently reflects off the upper guidewall and the shear layer and causes considerable bending of the shear layer in the process. Nevertheless, the visual shear layer thickness at the downstream location is within 5% of the nominal case 3 flow. Note also that some large-scale structure is apparent in this example.

Figure 11b shows another off-design case 3 flow, although here the strength of the wave coming off the splitter tip is much weaker than in Fig. 11a; nevertheless, this shear layer possesses considerable large-scale, two-dimensional structure. It should be emphasized that these structures were not seen in the normal pressure-matched flows, suggesting that the planar wave from the splitter tip enhanced the formation of two-dimensional structure in the shear layer, perhaps by means of a resonant forcing mechanism. It should be noted that relatively few of the off-design flows, for which data are available, demonstrated such enhanced two-dimensional structure, attesting to the difficulty in achieving the required resonance conditions.

Conclusions

Nonreacting compressible turbulent shear layers were studied in a new blowdown facility. Side-view schlieren photographs of the high-compressibility flows [$M_{c1}^{(i)} = 0.90, 0.96$] revealed the presence of traveling shock and expansion waves in the low-speed fluid, waves created by unseen shear layer structures convecting at supersonic Mach numbers. The measured convection velocities of these structures are considerably higher than those predicted by models of isentropic pressure recovery at stagnation points in the convective frame. To the extent that large-scale structure appears, it is not as conspicuous as in incompressible shear layers. Generally, no large-scale structure is discernable in the early part of the flow in the present data, with some evidence for it at the downstream end. For $M_{c1}^{(i)} > 0.3$, the measured shear layer growth rates agree with previous results by other experimenters. For $M_{c1}^{(i)} < 0.3$, a curious branch in normalized growth rate was observed. Finally, it was observed that the shear layer growth rate was not affected significantly by the impact of strong planar waves created by a pressure mismatch at the splitter tip.

Acknowledgments

The fabrication of the facility and the research described in this paper were sponsored by the Air Force Office of Scientific Research, Contract F49620-86-C-0134, and Grants 88-0155 and 90-0304. The authors would like to acknowledge the many people at California Institute of Technology who contributed to the design, construction, and operation of the new facility used in this work. Particular thanks go to Dimitri Papamoschou and Cliff Frieler for design contributions and many discussions, to Earl Dahl for assistance above and beyond the call of duty, to Dan Lang for his contributions and integration of the active pressure control system, as well as the electronics and data acquisition system in general, and to Chris Bond for his help in running the experiments.

References

[1]Chinzei, N., Masua, G., Komuro, T., Murakami, A., and Kudou, K., "Spreading of Two-Stream Supersonic Turbulent Mixing Layers," *Physics of Fluids,* Vol. 29, No. 5, 1986, pp. 1345–1347.

[2]Papamoschou, D., and Roshko, A., "The Compressible Turbulent Shear Layer: An Experimental Study," *Journal of Fluid Mechanics,* Vol. 197, Dec. 1988, pp. 453–477.

[3]Papamoschou, D., "Structure of the Compressible Turbulent Shear Layer," *AIAA Journal,* Vol. 29, No. 5, 1991, pp. 680, 681.

[4]Clemens, N. T., and Mungal, M. G., "Two- and Three-Dimensional Effects in the Supersonic Mixing Layer," AIAA Paper 90-1978, July 1990.

[5]Clark, R. L., Jr., Ng, W. F., Walker, D. A., and Schetz, J. A., "Large-Scale Structure in a Supersonic Slot-Injected Flow Field," *AIAA Journal,* Vol. 28, No. 6, 1990, pp. 1045–1051.

[6]Fourguette, D., Mungal, M. G., and Dibble, R., "Time Evolution of the Shear Layer of an Axisymmetric Supersonic Jet at Matched Conditions," AIAA Paper 90-0508, Jan. 1990.

[7]Dutton, J. C., Burr, R. F., Goebel, S. G., and Messersmith, N. L., "Compressibility and Mixing in Turbulent Free Shear Layers," *12th Symposium on Turbulence* (preprint), Univ. of Missouri—Rolla, Rolla, MO, Sept. 1990.

[8]Bogdanoff, D. W., "Compressibility Effects in Turbulent Shear Layers," *AIAA Journal,* Vol. 21, No. 6, 1983, pp. 926, 927.

[9]Dimotakis, P. E., "Two-Dimensional Shear-Layer Entrainment," *AIAA Journal,* Vol. 24, No. 11, 1986, pp. 1791–1796.

[10]Coles, D., "Dryden Lecture: The Uses of Coherent Structure," AIAA Paper 85-0506, Jan. 1985.

[11]Dimotakis, P. E., "Turbulent Free Shear Layer Mixing and Combustion," *High Speed Flight Propulsion Systems,* edited by S. N. B. Murthy and E. T. Curran, Vol. 137, Progress in Astronautics and Aeronautics, AIAA, Washington, DC, 1991, Chap. 5, pp. 265–340.

[12]Dimotakis, P. E., "On the Convection Velocity of Turbulent Structures in Supersonic Shear Layers," AIAA Paper 91-1724, June 1991.

[13]Hall, J. L., "An Experimental Investigation of Structure, Mixing and Combustion in Compressible Turbulent Shear Layers," Ph.D. Thesis, California Inst. of Technology, Pasadena, CA, 1991.

[14]Brown, G. L., "The Entrainment and Large Structure in Turbulent Mixing Layers," *Proceedings of the 5th Australasian Conference on Hydraulics and Fluid Mechanics,* Univ. of Canterbury, Christchurch, New Zealand, 1974, pp. 352–359.

[15]Lowson, M. V., and Ollerhead, J. B., "Visualization of Noise from Cold Supersonic Jets," *Journal of the Acoustical Society of America,* Vol. 44, No. 2, 1968, p. 624.

[16]Tam, C. K. W., "Directional Acoustic Radiation from a Supersonic Jet," *Journal of Fluid Mechanics,* Vol. 46, Pt. 4, 1971, pp. 757–768.

[17]Oertel, H., "Mach Wave Radiation of Hot Supersonic Jets Investigated by Means of the Shock Tube and New Optical Techniques," *Proceedings of the 12th International Symposium on Shock Tubes and Waves,* Magnes, Jerusalem, 1980, pp. 266–275.

[18]Lessen, M., Fox, J. A., and Zien, H. M., "On the Inviscid Stability of the Laminar Mixing of Two Parallel Streams of a Compressible

Fluid," *Journal of Fluid Mechanics,* Vol. 23, Pt. 2, 1965, pp. 355–367.

[19]Gropengiesser, H., "Study of the Stability of Boundary Layers in Compressible Fluids," NASA-TT-F-12786, Feb. 1970, p. 786.

[20]Ragab, S. A., and Wu, J. L., "Linear Instabilities in Two-Dimensional Compressible Mixing Layers," *Physics of Fluids A,* Vol. 1, No. 6, 1989, pp. 957–966.

[21]Zhuang, M., Kubota, T., and Dimotakis, P. E., "Instability of Inviscid, Compressible Free Shear Layers," *AIAA Journal,* Vol. 28, No. 10, 1990, pp. 1728–1733.

[22]Zhuang, M., Dimotakis, P. E., and Kubota, T., "The Effect of Walls on a Spatially Growing Supersonic Shear Layer," *Physics of Fluids A,* Vol. 2, No. 4, 1990, pp. 599–604.

[23]Brown, G. L., and Roshko, A., "On Density Effects and Large Structure in Turbulent Mixing Layers," *Journal of Fluid Mechanics,* Vol. 64, Pt. 4, 1974, pp. 775–816.

[24]Frieler, C. E., and Dimotakis, P. E., "Mixing and Reaction at Low Heat Release in the Non-Homogeneous Shear Layer," First National Fluid Dynamics Congress, Paper 88-3626, July 1988.

[25]Dimotakis, P. E., and Brown, G. L., "The Mixing Layer at High Reynolds Number: Large-Structure Dynamics and Entrainment," *Journal of Fluid Mechanics,* Vol. 78, Pt. 3, 1976, pp. 535–560 + 2 plates.

[26]Koochesfahani, M. M., and Frieler, C. E., "Instability of Nonuniform Density Free Shear Layers with a Wake Profile," *AIAA Journal,* Vol. 27, No. 12, 1989, pp. 1735–1740.

[27]Lu, G., and Lele, S. K., "A Note on the Density Ratio Effect on the Growth Rate of a Compressible Mixing Layer," *Physics of Fluids A* (submitted for publication).